



Exploring the use of Unmanned Aerial Vehicles (UAVs) with the simplified 'triangle' technique for soil water content and evaporative fraction retrievals in a Mediterranean setting

George P. Petropoulos , Antonino Maltese , Toby N. Carlson , Giuseppe Provenzano , Andrew Pavlides , Giuseppe Ciralo , Dionissios Hristopoulos , Fulvio Capodici , Christos Chalkias , Gino Dardanelli & Salvatore Manfreda

To cite this article: George P. Petropoulos , Antonino Maltese , Toby N. Carlson , Giuseppe Provenzano , Andrew Pavlides , Giuseppe Ciralo , Dionissios Hristopoulos , Fulvio Capodici , Christos Chalkias , Gino Dardanelli & Salvatore Manfreda (2021) Exploring the use of Unmanned Aerial Vehicles (UAVs) with the simplified 'triangle' technique for soil water content and evaporative fraction retrievals in a Mediterranean setting, International Journal of Remote Sensing, 42:5, 1623-1642, DOI: [10.1080/01431161.2020.1841319](https://doi.org/10.1080/01431161.2020.1841319)

To link to this article: <https://doi.org/10.1080/01431161.2020.1841319>



Published online: 24 Nov 2020.



Submit your article to this journal [↗](#)



Article views: 100



View related articles [↗](#)



View Crossmark data [↗](#)



Exploring the use of Unmanned Aerial Vehicles (UAVs) with the simplified 'triangle' technique for soil water content and evaporative fraction retrievals in a Mediterranean setting

George P. Petropoulos^a, Antonino Maltese^b, Toby N. Carlson^c, Giuseppe Provenzano^d, Andrew Pavlides^a, Giuseppe Ciralo^b, Dionissios Hristopoulos^e, Fulvio Capodici^b, Christos Chalkias^f, Gino Dardanelli^b and Salvatore Manfreda^g

^aSchool of Mineral Resources Engineering, Technical University of Crete, Crete, Greece; ^bDepartment of Engineering, Università Degli Studi di Palermo, Palermo, Italy; ^cDepartment of Meteorology, Penn State University, University Park, PA, USA; ^dDepartment of Agriculture, Food and Forest Sciences (SAAF), Università Degli Studi di Palermo, Palermo, Italy; ^eSchool of Electrical & Computer Engineering, Technical University of Crete, Crete, Greece; ^fDepartment of Geography, Harokopio University of Athens, Athens, Greece; ^gDipartimento di Ingegneria Civile, Edile e Ambientale (DICEA), Università Degli Studi di Napoli Federico II, Napoli, Italy

ABSTRACT

Information acquired from Unmanned Aerial Vehicles (UAVs) is frequently used nowadays in a variety of disciplines and research fields. The present study explores for the first time the combined use of UAVs with a newly proposed technique for estimating evaporative fraction (EF) and surface soil moisture (SSM). The investigation is performed in a typical Mediterranean setting, a citrus field with flat topography divided in two plots with different irrigation schemes, in Sicily, Italy, at which ground data acquired during an extensive field campaign in July 2019. Reasonable estimates of both EF and surface wetness were produced, with patterns in agreement to vegetation cover fragmentation, topography, and other site-specific characteristics. Validation shows average error of 0.053 for EF and of $0.040 \text{ cm}^3 \text{ cm}^{-3}$ for SSM. The results are comparable or better to those reported in analogous studies performed in similar areas. This implies that the investigated approach performs well under the semi-arid conditions characterizing the experimental set up. To our knowledge, this study represents the first evaluation of the combined use of the 'simplified triangle' with very high-resolution UAV imagery. As such, the findings are of significance regarding the potential future use of the 'simplified triangle' approach particularly with very fine resolution imagery such as that provided by UAV for mapping and monitoring EF and SSM in agricultural and natural ecosystems.

ARTICLE HISTORY

Received 22 July 2020

Accepted 27 September 2020

1. Introduction

The natural processes taking place on the Earth's surface control the energy and mass exchanges between land and atmosphere and are key drivers of the Earth's system (North

CONTACT : George P. Petropoulos  petropoulos.george@gmail.com; gpetropoulos@hua.gr  School of Mineral Resources Engineering, Technical University of Crete, Crete 73100, Greece

© 2020 Informa UK Limited, trading as Taylor & Francis Group

et al. 2015; Gerken, Ruddell, and Yu et al. 2019). Today, particularly so in light of climate change and concerns related global food and water security, an improved understanding of land-atmosphere interactions is a topic of urgent importance (Ireland et al. 2015; Deng et al. 2019). In this context, obtaining accurate information on the spatial and temporal variability of land surface parameters such as evaporative fraction, EF (defined as the ratio of instantaneous latent heat flux (LE) to net radiation (R_n) and surface soil moisture (SSM) is of primary interest for several environmental applications and research investigations (Jung et al., 2011; Srivastava et al. 2019). This is due to the influence of these parameters on key physical processes and feedback loops of the Earth system (Nutini et al., 2104; Srivastava et al. 2015; Amani et al. 2016). Accurate information on their spatiotemporal variability, particularly at fine spatial and temporal resolution, can provide valuable information in research studies and practical applications linked to ecosystem processes, plant water requirements and water resources management (Shi et al., 2014; Minacapilli et al. 2016; Deng et al. 2019; Yang et al., 2020).

Despite their significance, it is quite difficult to quantify EF and SSM on a routine basis over large geographical regions using ground instrumentation. The main reasons include the large spatiotemporal variability of these parameters (Bao et al. 2018). Earth Observation (EO) presents a suitable alternative to ground observations for deriving SSM and/or EF over large regions and diverse geographical scales (Tian et al. 2014). A variety of approaches have been proposed for this purpose, ranging from semi-empirical to physically-based ones (see Petropoulos, Ireland, and Barrett 2015; Petropoulos et al. 2018). Those approaches are characterized by different degree of complexity, input parameters requirements and retrieval accuracy.

A specific group of EO-based techniques commonly termed as surface temperature (T_s) and vegetation index (VI) methods (T_s/VI), has shown an excellent promise at deriving spatially explicit maps of sensible and latent heat fluxes (H, LE) and/or SSM. These methods utilize optical (visible and infrared – VNIR) and thermal infrared (TIR) EO data and are based on physical relationships between the satellite-derived T_s and a VI, the latter being associated to the existent degree of vegetation (Zhang et al. 2014; Capodici et al. 2020). If these parameters are in a scatter plot, provided that there is a full variability in VI, a triangular/trapezoidal shape similar to that shown in Figure 1 emerges. This shape, characterized by the physical boundaries also shown in Figure 1, results from the T_s sensitivity to water content, which increases as a function of the proportion of bare soil exposed. The biophysical properties included in this T_s/VI domain are well-documented (Gillies et al. 1997; Chauhan, Miller, and Ardanuy 2003; Maltese et al. 2015; Wang et al. 2018; Cui et al. 2020). Detailed descriptions of these properties, including the key parameters affecting the T_s/VI scatterplot shape, are summarized in Petropoulos et al. (2009) and Petropoulos et al. (2018). Tang et al. (2017) introduced the End-member-based Soil and Vegetation Energy Partitioning model (ESVEP), a two-source approach for estimating land surface evapotranspiration (ET) for which two dry edges could be considered in the case of a root zone water stress occurs. It is based on the consideration that soil evaporation primarily draws water from the upper soil layer, whereas, transpiration exploits water from the root zone. The temporal response of soil water content of the upper soil and root zone in the framework of the ET process is, therefore, different: the dynamic of the soil water content is more rapid in the upper layer; it is slower in the root zone.

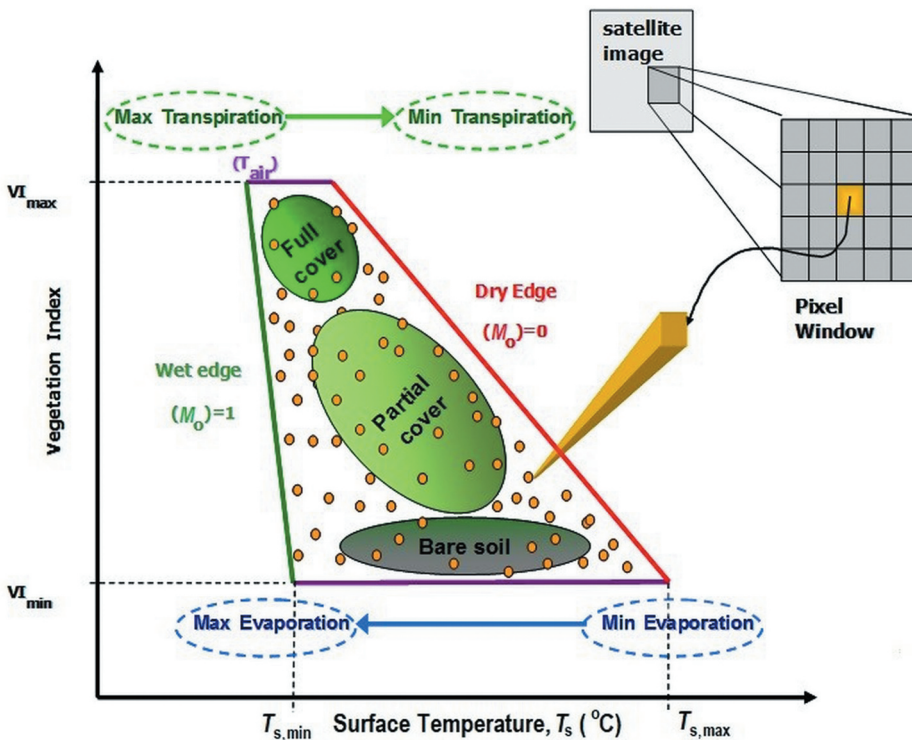


Figure 1. Conceptualization of the main properties encapsulated in a T_s/VI scatterplot (adopted from Petropoulos et al. 2009).

Recently, Carlson and Petropoulos (2019) proposed a T_s/VI technique for estimating both EF and SSM, which they named 'simplified triangle'. This approach is essentially a variant of the so-called 'triangle' technique (Carlson 2007) and does not require for its implementation a land biosphere model or any other ancillary data. These characteristics make this approach easy to apply in comparison to other T_s/VI methods. Furthermore, being dependent on a small number of easily computed EO-based parameters, it becomes a very attractive choice for potential operational use. Fuzzo et al. (2020) demonstrated how this newly introduced approach can be coupled with a crop prediction and a climatological water balance model in soybean yield prediction using MODIS data. However, as the technique is recent, studies validating its performance in different environments and with a range of EO instruments are scarce.

To our knowledge, this newly proposed technique has not been implemented on and verified for unmanned aerial vehicles (UAVs) data yet. UAV platforms with on-board visible/near infrared and thermal sensors have very important advantages over satellite EO platforms, such as user flexibility to select the target area and the frequency of data acquisition (Dawson et al. 2019; Liu et al. 2020). Therefore, this technique implementation with UAVs would be indisputably of key importance, as it would inform on its potential usefulness in a broad spectrum of practical applications and research purposes alike.

In this context, this study aims at exploring for the first time the combined use of the 'simplified triangle' with very high spatial resolution UAV data, to predict the spatio-

temporal variability of both EF and SSM. For this purpose UAV, ground truthing and ancillary data acquired during a field campaign that took place in July 2019 at one experimental site in Sicily, Italy, are employed. The experimental set up description is provided in Section 2, whereas the 'simplified' technique implementation with the UAV data is made available in Section 3, followed by the results and the related discussion which are described in Sections 4, and 5, respectively.

2. Materials

2.1. Study site

The study site is a citrus orchard field (*C. reticulata* Blanco, cv. Tardivo di Ciaculli) located in the neighbourhood of Palermo, Italy ($38^{\circ} 4'53.4''\text{N}$, $13^{\circ} 25' 8.2''\text{E}$). The site contains 30 year old tangerine trees planted at a regular spacing of 5.0 m \times 5.0 m (plant density of 400 plants per ha) and irrigated with a subsurface drip system. The area is in a typical eastern Mediterranean semi-arid environment. The study area has flat topography with elevation between 30 and 35 m above sea level, and slopes ranging from 1% to 4%.

To differentiate irrigation management, the field has been divided into two plots of about 4,000 m² each, as shown in Figure 2. The first plot was maintained under full irrigation (FI), whereas the second under deficit irrigation (DI) applied throughout phase II of fruit growth (from 1 July 2019 to 20 August 2019). Each plot was, in turn, divided into four sub-plots differentiated for the anti-root agents introduced into the emitters during the manufacturing process, but not for the irrigation management, nor for the emitters' hydraulic performance. The subsurface drip system is characterized by two lateral pipes per plant row, installed at a distance of 1.1 m from the trees and buried at a depth of 0.30 m. In each lateral pipe, self-compensating emitters were installed with half-metre spacing between them, nominal flow rate of 2.3 h⁻¹ and operating pressure of 150 kPa. A disc filter, an electric control valve, a relief valve, a pressure gauge, and a flow metre completed each sub-plot irrigation unit.

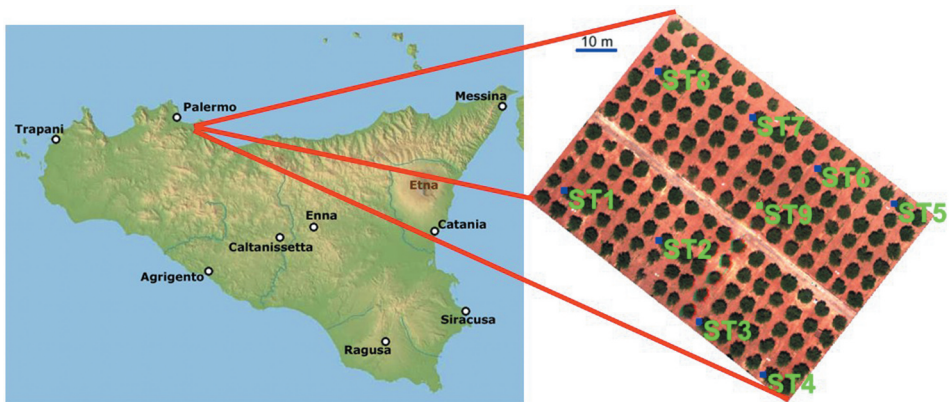


Figure 2. The experimental site, including the distribution of the ground measurement stations. ST1-8 refers to the locations of the probes that monitor soil water content, whereas ST9 is the eddy covariance system location. The image on the right is the actual UAV area covered by the UAV upon completion of orthorectification (see section 2.2.2 below).

The experimental setup is equipped with a WatchDog 2000 weather station (Spectrum Technologies, Inc.), including sensors for relative air humidity, wind speed and direction, air temperature, solar radiation, and rainfall, as well as eight 'drill & drop' frequency domain reflectometry sensors (Sentek Pty Ltd, Stepney, Australia) to monitor soil water content, installed on a central tree of each sub-plot, 0.30 m away from the closest emitter. All the sensors were interfaced with a communications board that uses the cellular 3 G data network for internet connection using the MODBUS RTU protocol to transfer and save the data into a MySQL database operated by AgriNET/Tuctronics which is accessible from the web. The system allows the download of weather variables, soil water content (SWC) and temperatures (T) in the root zone, at 10 cm intervals from the first 5 cm of the soil layer down to a depth of 0.6 or 1.2 m. The Scholander chamber (Scholander et al. 1965) was used to follow the temporal dynamic of predawn and midday stem water potential, whereas a couple of Granier thermal dissipation probes (Granier 1985) was installed in four trees to monitor sap flow during the irrigation season.

In addition, an eddy covariance flux tower was set up in the orchard in February 2019 to measure the turbulent fluxes (sensible, H, and latent, LE, heat fluxes) and a four-component net radiometer was used to measure net radiation (R_n) individual components. A CNR1 four component Net Radiometer was installed at 3.1 m a.g.l, while an InfraRed Gas Analyser IRGA LI7500 (manufactured by LI-COR, Inc.) and a CSAT3 Three Dimensional Sonic Anemometer anemometer (manufactured by Kipp & Zonen B.V.) were installed slightly above, at 3.5 m above ground level (a.g.l.), i.e. approximately 55 and 95 cm above the vegetation canopy. All the data were processed at 30 minutes interval. The footprint flux tower was calculated according to Schuepp et al. (1990) at 70% of the fluxes.

2.2. Data acquisition & pre-processing

2.2.1. Data acquisition

The fieldwork for this study was carried out on July 2019. A series of spatial and ancillary data was acquired on 30 July 2019 as part of the field campaign that was conducted in order to support the study implementation. In particular:

- **Global Navigation Satellite System (GNSS) Survey.** Nine black and white control targets, and the same number of aluminium targets were distributed on a regular grid to cover the whole study area.

The coordinates of the targets were measured by a NRTK survey using a Topcon Hiper V receiver (both Global Positioning System (GPS) and Glonass constellations). A UNIPA (University of Palermo) GNSS Cross-origin resource sharing (CORS) network encompassing 8 permanent stations, 2 of them installed on two University buildings in Palermo and Agrigento and 6 at other public institutions of the Sicilian territory was employed for Network real-time kinematic (NRTK) positioning. The network covers about 7400 km² western Sicily. The GNSS CORS Network project was carried out with the technical collaboration of Topcon Italy (that supported the scientific research with GNSS receivers and antennae), in the framework of developing a network for technical (real-time) and scientific (post-processing) use. The CORSs is included in the Topcon Netgeo GNSS network. Since 2013 the data retrieved from

UNIPA GNSS CORS network have been used for the computation of the RDN2 (*Rete Dinamica Nazionale 2*) which provides the WGS84 datum for Italy in the European Permanent Network (EPN subnetwork). UNIPA GNSS CORS network has received the scientific acknowledgment through many experiments in various application fields (Catania et al. 2020; Angrisano et al. 2020; Kenyeres et al. 2019; Pipitone et al. 2018; Dardanelli et al. 2015, 2014,; Dardanelli and Carella 2013). Since 2013 the post-processing RINEX (Receiver INdependent EXchange) data have been made available for the evaluation of the national reference framework by the IGMI (Italian cartographic military institute) and for technical researches able to investigate the horizontal and vertical velocity map in Italy (Maseroli 2015). NRTK positioning was carried out using the hardware and software infrastructure of the permanent Netgeo-Topcon Italy network framed in the reference system ETRF2000 (powered by UNIPA GNSS CORS) and in particular via the VRS (Virtual Reference Station) stream. Data availability and geodetic framework are described in Dardanelli, Lo Brutto, and Pipitone (2020). The processing of GNSS data acquired to allow an accurate orthorectification of multi-spectral and thermal images was carried out by Meridiana software ver. 2020.

- **Proximity sensing images.** Multispectral images were acquired using a NT8 contras octocopter carrying a RikolaDT-17 Fabry-Pérot camera (manufactured by Rikola Ltd). The multispectral camera has a 36.5° Field of View. It was set-up to acquire images in 9 spectral bands with a 10 nm bandwidth. Central wavelengths were 460.43, 480.01, 545.28, 640.45, 660.21, 700.40, 725.09, 749.51 and 795.53 nm. At a flight altitude of 50 m above ground (a.g.l.), the average Ground Sampling Distance (GSD) was 3 cm. Thermal images were acquired almost simultaneously to the multispectral images, using a DJI Mavic 2 Enterprise Dual quadcopter carrying on-board a FLIR Lepton® (manufactured by FLIR® Systems, Inc) acquiring in the longwave infrared spectral range (from 8 to 14 μm), with a thermal sensitivity lower than 50 mK (0.050°C). The average GSD was 3.46 cm. All the images were resampled at 4 cm spatial resolution using a pixel aggregate resampling method.
- **Spectroradiometric measurements.** Four reference targets, ranging in a greyscale from black to white were also positioned to allow the spectral reflectance calibration by means of a field spectroradiometer. The employed ASD FieldSpec®FR spectroradiometer (Analytical Spectral Device, ASD, Inc.) measured the full solar spectrum (between 350 and 2500 nm) with no fore optic attached.
- **Thermographs.** Ground measurements of surface temperature (T_s) were carried out at noon using a handheld FLIR SC660 (FLIR® Systems, Inc.) characterized by a sensitivity lower than 30 mK.

2.2.2. Pre-processing

Following the data acquisition, standard pre-processing steps were applied. To orthorectify the multispectral and thermal images, a standard photogrammetric/SfM approach (e.g. Harwin and Lucieer 2012) was applied via Pix4D mapper (by Pix4D Inc.). A Topcon Hiper V receiver (both GPS and GNSS Connectivity) was employed to acquire ground control points for the orthorectification. The average position dilution of precision (PDOP) and the geometric dilution of precision (GDOP) were 1.8 and 2.0, respectively. The control targets were positioned with average planimetric and altimetric accuracy of ± 2 cm that can be considered within acceptable geometrical configuration limits to orthorectify the

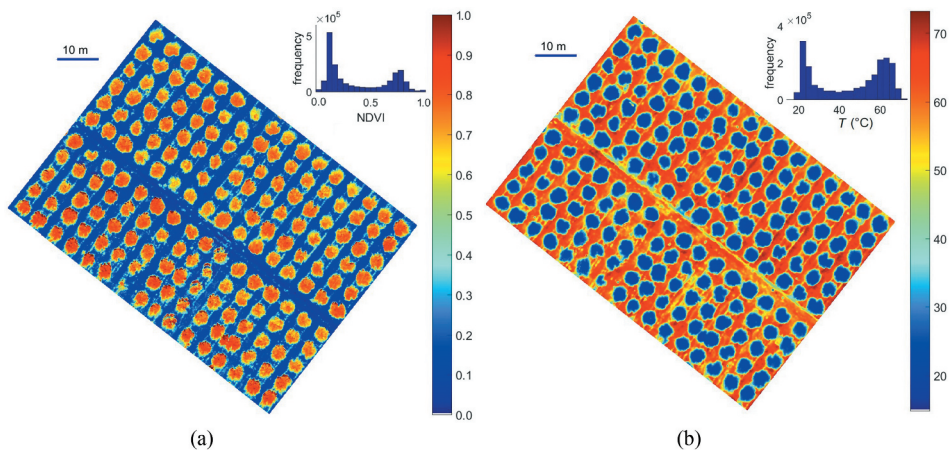


Figure 3. Pseudo colour maps of NDVI (a) and T_s (°C) (b) derived upon completion of the pre-processing steps. The insets show the frequency histograms of NDVI and T_s respectively. Temperature units are in Celsius.

UAV images, considering that these latter are characterized by a spatial resolution of 4 cm once orthorectified. Images acquired in the visible and near infrared were calibrated to ground reflectance implementing the empirical line technique (Karpouzli and Malthus 2003), which allows the simultaneous correction of the atmospheric influence. Similarly, TIR images were calibrated into surface radiometric temperatures by means of a linear regression with at ground thermographs and an emissivity map of the soil vegetation system (Negm et al. 2017). The spatial distribution of emissivity was calculated according to Valor and Caselles (1996). Given the spatial resolution of the images (about 10^{-2} m) compared to the spacing of the trees (about 5 m) we did not consider the cavity effect. We assume the emissivity values for bare soil and densely vegetated ground to be equal to 0.97 and 0.99, respectively, as reported in Sobrino, Jimenez-Munoz, and Paolini (2004). Figure 3 illustrates the Normalized Difference Vegetation Index (NDVI) and of Surface Temperature (T_s) final products upon completion of all pre-processing steps.

3. Methods

3.1. Simplified triangle method

A comprehensive account of the ‘simplified’ triangle technique implementation is available in Carlson and Petropoulos (2019). Briefly, the method allows the retrievals of two parameters, the soil water availability (M_o) and EF. M_o represents surface wetness in the bare soil surface (top few millimetres of it) and it is computed from the ratio between the actual soil/vegetation system evapotranspiration ET and potential evapotranspiration (ET/ET_p). M_o is also equated to SSM by multiplying M_o with the soil’s field capacity. On the other hand, EF is defined as the ratio between latent heat flux (LE) and net radiation (R_n).

EF and M_o are obtained from the T_s/VI feature space. The scatterplot is constructed by plotting the T_s versus fractional vegetation (F_v), where the latter is computed from the NDVI (see Equation (1) below) and its corresponding range of variability, as proposed by

Carlson (2007). Upon completion of this step, a number of parameters need to be determined, namely: (a) the NDVI values for bare soil and dense vegetation (respectively, $NDVI_0$ and $NDVI_s$), and (b) the highest value of T_s (T_s [max]) which is characteristic of dry/bare soil pixels, as well as the minimum value of T_s (T_s [min]).

$NDVI_0$, $NDVI_s$, T_{max} and T_{min} are used to specify the T_s/VI feature space boundaries and to constrain the solution for EF and M_o . $NDVI_s$ and T_{min} represent dense vegetation and define the lower left (wet) vertex of the triangle, i.e. the so-called ‘wet edge’ or ‘cold edge’ (see Figure 4). The wet edge corresponds to M_o and EF values equal to 1.0. Similarly, $NDVI_0$ and T_{max} define the lower right vertex of the triangle, the so-called ‘dry edge’ or ‘warm edge’ (also shown also in Figure 4). These points characterize the soil dryness boundary with $M_o = 0$ and covers the area from T_{max} and $NDVI_0$ to $NDVI_s$, which, for a triangle with a distinct upper vertex, occurs at T_{min} . Even though $M_o = 0$ along the ‘dry edge’, along the dry edge EF itself is non-zero apart from the triangle’s lower right vertex. The next step in the technique implementation includes the scaling of T_s to T^* (by applying Equation (2) below), which ranges between zero to one.

At this stage two central hypotheses are made. The first is that when vegetation is at wilting point transpiration is always equal to the potential transpiration, as generally assumed in nearly all T_s/VI approaches (e.g. Jiang and Islam 2003). The second hypothesis is related to the relationship between EF and M_o within the T_s/VI domain, which is assumed to be linear.

Thus, on the basis of the assumptions above, M_o is defined as the ratio between the lengths ‘a’ and ‘d’. Both these lengths depend on T^* and F_r . For conditions where a pixel comprises of both areas of vegetation and bare soil, the canopy EF is taken as the weighted value of EF for the vegetation fraction of the pixel ($EF_{veg} = 1$, by definition). As such, both M_o and EF are computed for all pixels contained in the T^*/F_r domain from the implementation of Equations (3) and (4) shown below.

$$F_r = \left\{ \frac{(NDVI) - (NDVI_0)}{(NDVI_s) - (NDVI_0)} \right\}^2 \tag{1}$$

$$T^* = \{T - T_{min}\} / \{(T_{max} - T_{min})\} \tag{2}$$

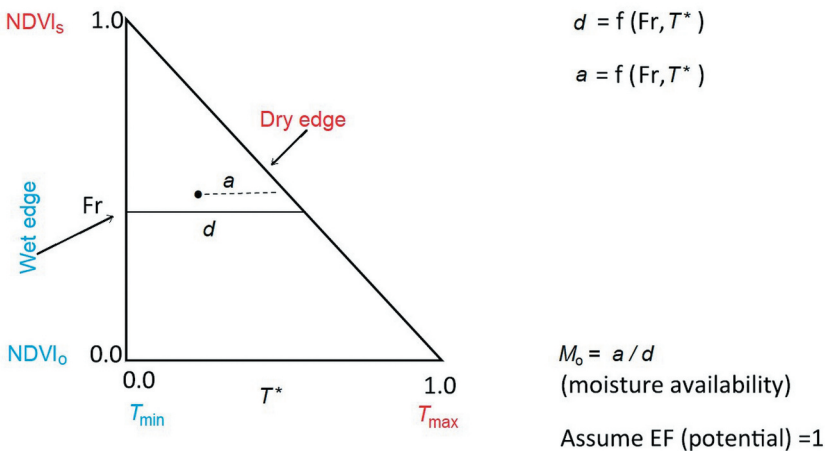


Figure 4. Graphical summary of the ‘simplified’ triangle method principles and critical points selection required in its implementation (adopted from Carlson and Petropoulos 2019).

$$M_o = 1 - T^*(\text{pixel})/T^*(\text{dry edge}) \quad (3)$$

$$EF = (EF_{\text{soil}})(1 - F_r) + F_r (EF_{\text{veg}}) = M_o(1 - F_r) + F_r \quad (4)$$

In the above, EF_{soil} refers to the ratio between soil evaporation and net radiation. $T(\text{pixel})$ is the scaled surface temperature T^* for a given pixel within the scatterplot and $T(\text{dry edge})$ is the value of T^* at the dry edge of the triangle. In this study, the values for the temperature limits were $T_{\text{min}} = 19.40$ °C and $T_{\text{max}} = 73.27$ °C, whereas for NDVI were $NDVI_0 = 0$ and $NDVI_1 = 1$. Noticeably that fully vegetated pixels exhibit a variability in T^* of 0.25 conferring to the $T^* - F_r$ scatterplot a trapezoidal shape. The variability in T^* could be attributed to the very high spatial resolution achieved by UAV which allows to record the surface temperatures of the single leaves of the same canopy. In particular, the variability in T^* is attributed to the different exposure to the direct solar radiation of the single leaves which controls i) directly, the individual leaf warming up; ii) indirectly, the leaf transpiration.

The implementation of the steps summarized above to the pre-processed UAV data resulted in the scatterplots of NDVI vs T_s and of computed F_r vs T^* shown in [Figure 5](#). The spatial maps of F_r and T^* are also shown in this figure.

3.2. Statistical analysis

Evaluation of the predicted SSM and EF included at first a visual inspection of the spatiotemporal variability of the derived maps. Next, the main validation approach involved comparisons at pixel level between the predicted and measured parameters. The statistical scores computed that quantify the agreement between predictions and observations are summarized in [Table 1](#). These statistical measures have already been used in similar past verification exercises (e.g. Nutini et al. 2014; Piles et al., 2016; Amani et al. 2016; Xu et al. 2018; Wang et al. 2018).

4. Results

4.1. Visual comparisons

The EF and SSM maps and their corresponding histograms obtained from the UAV data and the 'simplified triangle' technique are illustrated in [Figure 6](#). The first step of the analysis included a visual inspection of the spatial variability of the derived parameters. As can be observed, both EF and SSM maps exhibited a sensible range of values as well as reasonable spatial variability. Clearly, the spatial variability is in agreement with the changes in land use/cover, as well as with the derived F_r and T_s maps based on the UAV data that were presented in [Figure 5](#). Both EF and SSM predicted by the 'simplified' triangle are spatially consistent with the soil/vegetation cover patterns and variability: in particular, high values of both variables correspond to the vegetated areas of the image, whereas low values appear in areas of bare soil.

To further illustrate the above observation, it was further investigated the variability of the derived parameters separately for the bare soil and the partially or fully vegetated components (see [Figure 7](#)). As evidenced in the maps shown in [Figure 7](#) (and their associated histograms), the variability of the examined parameters is largely explained

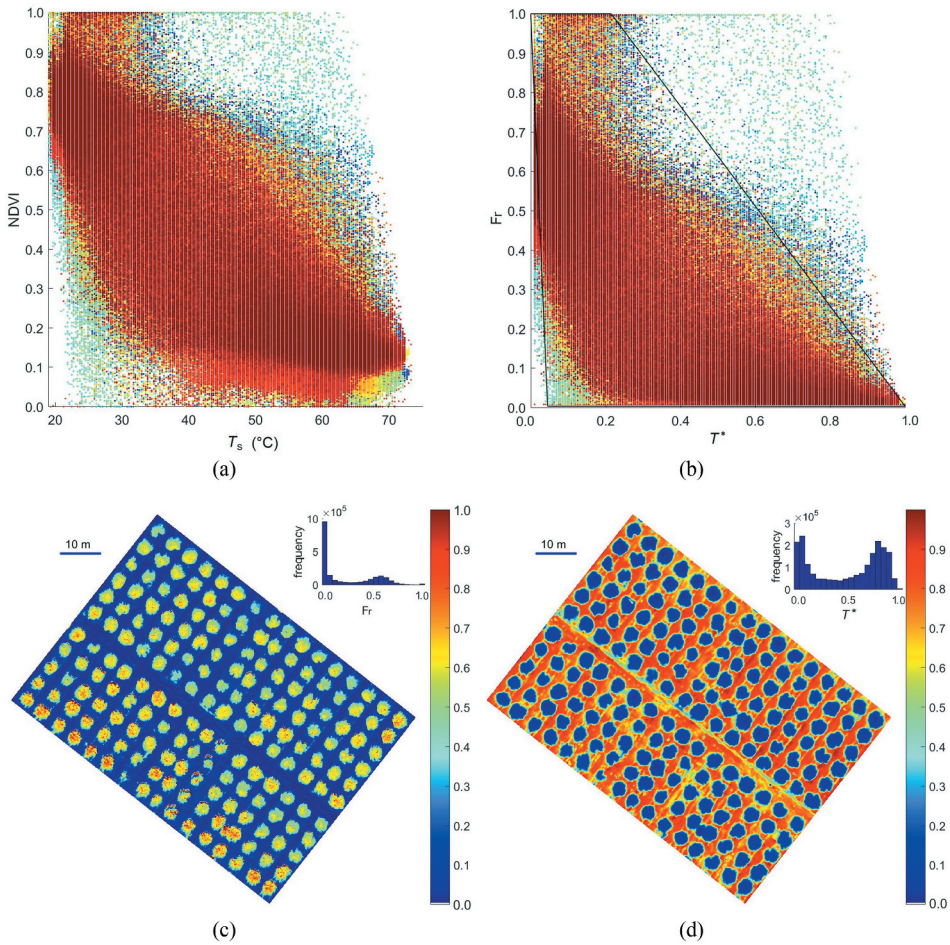


Figure 5. The scatterplots derived during the implementation (a,b), the F_r map (c) and the T^* map (d), derived from the datasets acquired with UAV. The ‘wet’ and ‘dry’ edge of the proposed triangle is shown by the continuous black line in scatterplot (b). The different colours in scatterplots (a,b) are for illustrative purposes only.

Table 1. Statistical measures used to assess the agreement between the predictions and ground observations. Subscripts $i = 1 \dots N$ refer to the individual observations, while O and P refer to the observed and predicted values.

Name	Description	Mathematical definition
Bias/MBE	Bias (accuracy) or Mean Bias Error	$\text{Bias} = \sum_{i=1}^N \frac{P_i - O_i}{N}$
Scatter/SD	Scatter (precision) or Standard Deviation	$S = \sqrt{\sum_{i=1}^N \frac{(P_i - O_i - (P_i - O_i))}{N}}^2$
RMSE	Root Mean Square Error	$\text{RMSE} = \sqrt{\sum_{i=1}^N \frac{(P_i - O_i)^2}{N}}$

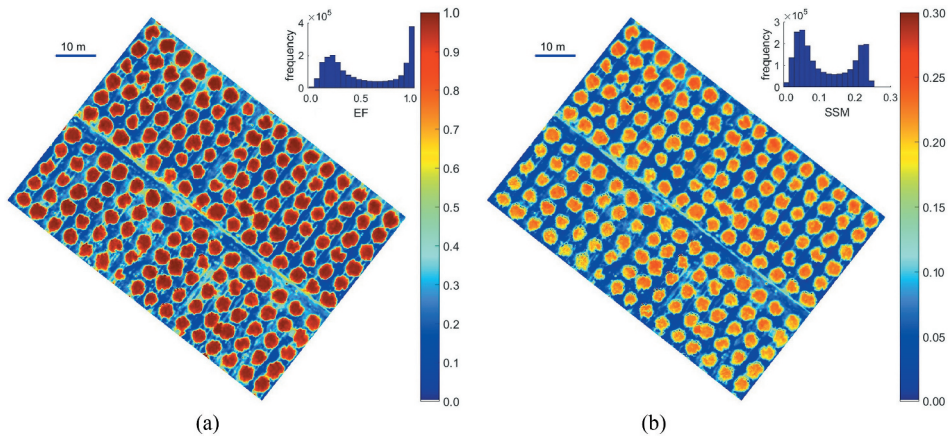


Figure 6. Maps of EF (a) and SSM (b) computed from the 'simplified triangle' implementation using the data retrieved with UAV. The corresponding histograms are also shown.

by the spatial variability in the land surface fragmentation. It is evident from the visual comparisons of bare soil and vegetation maps and histograms, that the variability of the vegetation for both EF and SSM is significantly higher in bare soil. From these figures it is shown that the EF and SSM for vegetation are predominantly above 0.9 EF and 0.2 SSM. Bare soil presents higher variability, but the highest frequencies (especially for SSM) are close to 0.26.

The last step of the visual analysis focused on an arbitrary transect, chosen as the diagonal line connecting the North and the South vertices of the experimental site. The spatial evolution of each predicted parameter along this transect is depicted in Figure 8. This approach allows examining simultaneously the variability of the different parameters, namely of EF, SSM, F_r , and T^* . The results of this analysis are depicted in Figure 8. As one can notice, the variability of the predicted parameters within the field follows largely explainable trends, depending on both F_r and T^* . This observation provided further evidence of the technique's ability to satisfactorily predict both EF and SSM in the field when implemented with the UAV data.

4.2. Point comparisons

The results which concerned point-wise (i.e. pixel level) comparisons are summarized in Table 2. As already noted, ground measurements of the radiation and turbulent fluxes were acquired at a single location within the experimental field. On the other, SSM measurements were conducted at a total of eight sites across the field, in which two different irrigation strategies were applied since 1 July 2019. In particular, sites 1 to 4 were maintained under full irrigation, whereas sites 5 to 8 under water deficit conditions.

As can be observed (in Table 2), the 'simplified triangle' achieved very good predictions of both EF and SSM, which are in close agreement to the field observations and in the same range as the results of similar studies (e.g. Peng and Loew 2014; Bai, Zhang, and Meng 2019). The predicted EF value, compared with the observed one, was slightly overestimated, with an absolute difference of 0.053. However, it should be noted that

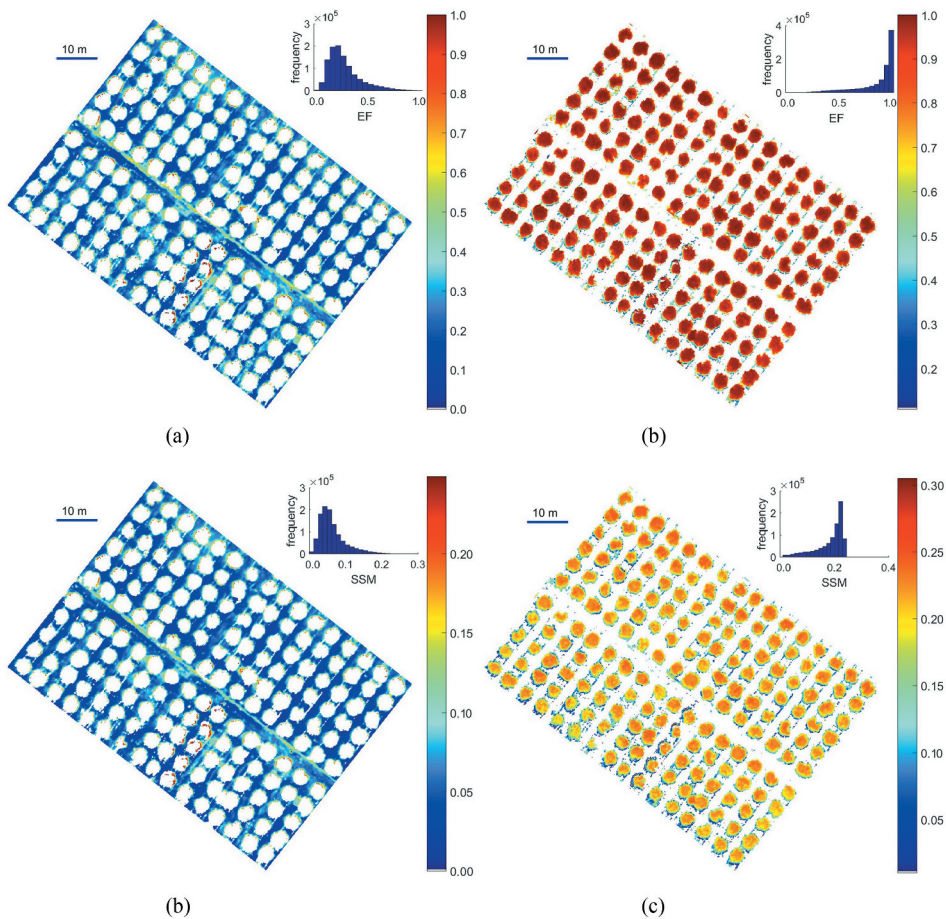


Figure 7. EF maps computed separately for the vegetated area (b) and for bare soil (a). Similarly, the derived SSM maps for the vegetated area (d) and for the bare soil (c), are also shown. Each map is accompanied by the corresponding frequency histogram.

this difference is also based on a single ground measurement, since there was only one eddy covariance station installed in the central part of the experimental site. In reference to the soil water content, Table 2 shows that the predicted SSM is in very good agreement with the respective measurements, with RMSE of 0.040 cm cm^{-3} . Scatter (0.031 cm cm^{-3}) contributes to RMSE relatively more than Bias ($-0.025 \text{ cm cm}^{-3}$) but not overly so.

As shown in Table 2, the mean predicted SSM (denoted as 'P') for the locations of Stations 1 to 4 (plots with full irrigation) is 0.123 cm cm^{-3} while for locations of stations 5 to 8 (plots with deficit irrigation) the mean predicted SSM is lower at 0.096 cm cm^{-3} . On the other hand, the measured SSM by the stations (denoted as 'O') does not reveal remarkable differences between plots maintained under different irrigation strategies. The mean observed SSM for plots 1 to 4 is $0.138 \text{ cm}^3 \text{ cm}^{-3}$, while for the plots 5 to 8 it is only marginally lower and equal to 0.131 cm cm^{-3} . While bias is generally low, the predicted SSM underestimates the corresponding values in all the plots under deficit

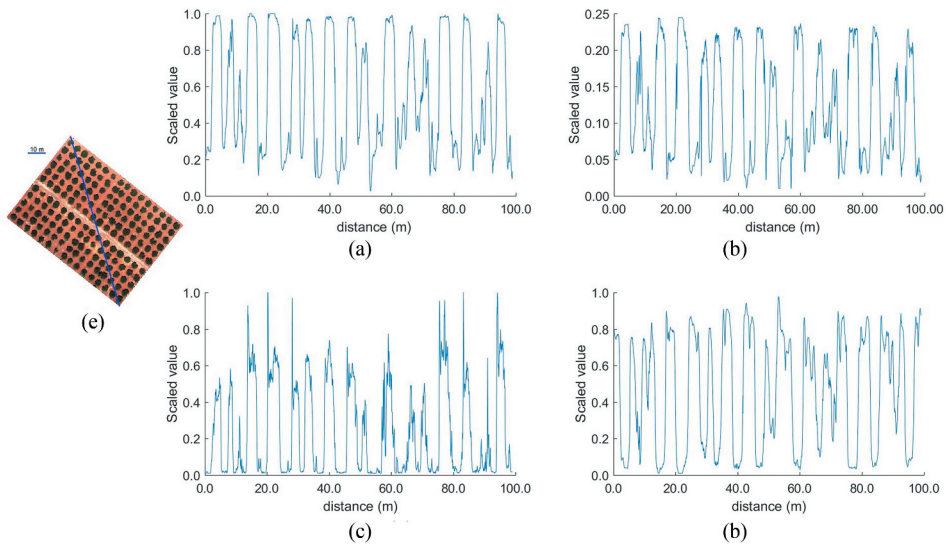


Figure 8. Arbitrarily selected transect within the field (e), and plots of the spatial variation of EF (a), SSM (b), F_r (c) and T^* (d) along the selected transect.

Table 2. Summary of the point by point comparisons between the ground observations (O) and the corresponding predicted with the 'simplified triangle' (P). The differences (D) between predicted and observed values are also indicated. Bias, Scatter and RMSE are expressed in units of $\text{cm}^3 \text{cm}^{-3}$.

Fluxes (-)	O	P	D
LE R_n^{-1}	0.266	0.319	0.053
SSM ($\text{cm}^3 \text{cm}^{-3}$)	0	P	D
SM1	0.139	0.090	-0.049
SM2	0.107	0.132	0.025
SM3	0.162	0.171	0.009
SM4	0.145	0.099	-0.045
SM5	0.078	0.073	-0.006
SM6	0.121	0.084	-0.037
SM7	0.145	0.084	-0.061
SM8	0.180	0.144	-0.036
	Bias		-0.025
	Scatter		0.031
	RMSE		0.040

irrigation by $-0.035 \text{ cm cm}^{-3}$ on average. However, for the fully irrigated plots, the underestimation is less than half in magnitude (equal to $-0.015 \text{ cm cm}^{-3}$). All in all, these results suggest that the 'simplified triangle' performed satisfactorily in predicting both the EF and SSM under the examined conditions.

5. Discussion

Based on the results obtained (Section 4), the 'simplified triangle' technique performed well to in reproducing the high spatial resolution of EF and M_o /SSM maps for the study area. Both predicted maps exhibited a largely explainable spatial variability across the

experimental site, with patterns in agreement to land cover type, topography and other site-specific characteristics. In terms of statistical agreement, prediction accuracy was good for both EF and SSM, and in agreement to the accuracies reported by other independent investigators using different approaches and EO data types. For EF the difference between the predicted and measured value is 0.053, giving a slight over-estimation. After the M_o was converted to SSM for the 8 stations, the results showed fairly low RMSE (0.040 cm cm^{-3}) and low underestimation (Bias = -0.025). These values are close to those reported by other studies retrieving EF and SSM using TIR-based techniques (e.g. Peng and Loew 2014; Nutini et al. 2014; Lu et al. 2015; Xu et al. 2018; Bai, Zhang, and Meng 2019). Thus, findings, although are based on the single image analysis, are confirming the usefulness of the examined technique for EF and SSM spatial determination at very fine resolution when implemented with UAV data.

There are a few factors which should be taken into consideration as well, when interpreting the statistical agreement found herein. For example, the accuracy of the retrieved F_r and of T_s is a possible cause of error as the technique requires only those two parameters as inputs for its implementation. In our study, LST was measured by FLIR SC660 with an error lower than $0.03 \text{ }^\circ\text{K}$, which is considered very small. Furthermore, since T_s is scaled in the 'triangle', the effect of the predicted temperature accuracy might be small (Carlson 2007). Possible reasons for the lack of complete agreement could be related to the scale-mismatch between the EO-data and the in-situ measurements, geo-location errors, and surface heterogeneity at the UAV sensor spatial resolution, even though in this particular case predictions were obtained at very high spatial resolution. Another possible factor concerning the SSM comparisons in particular is that the ground measurements were acquired at 0 to 10 cm depth, while the UAV-derived ones respond to soil water content at a much shallower layer (0 to 5 cm) over bare soil. Effective soil depth for SSM measurement is an issue under investigation (Amani et al. 2016). Some studies (Finn et al. 2011; Kasim, Carlson, and Usman 2020) suggest an effective measurement at a depth of 5 cm, while other studies suggest effective agreement at a depth of 10 cm. Furthermore, uncertainties due to the instrumentation accuracy for EF and R_n measurement should further be considered. Various studies have reported that errors in instantaneous LE flux measurement can be in the order of 20% to 30%, which can be even higher under certain circumstances (such as terrain features); similarly a measurement uncertainty for R_n of 10% is not uncommon (Petropoulos, Carlson, and Griffiths 2013).

Despite the promising results obtained in this first investigation performed herein, the 'simplified triangle' technique has some limitations which should also be acknowledged. Those include its requirement to have within the image field of view a sufficient variability of F_r and SSM range, in order to properly define the 'wet' edge and the 'dry' edge. Another issue is the possible human error in the selection of warm and cold edges. However, this is an issue common to other T_s/VI methods (Tomas et al. 2014; Mi et al. 2015). Furthermore, the technique assumes a linear relationship between the TS/VI feature space and the predicted EF and SSM, which might not necessarily be the case in nature.

Nonetheless, the 'simplified triangle' capitalizes on the inherent relationships existing in the T_s/VI feature space for estimating M_o and EF. Yet, it seems to have some strong advantages in comparison to other T_s/VI methods. The technique is simple to be applied and is dependent on a few input parameters which can be easily computed from EO sensors. This makes the technique implementation quick and computationally

inexpensive when that is to be applied to small scale studies. Its implementation, particularly with UAV images, presents several advantages. When the technique is implemented with UAV data cloud cover is not an issue (as UAVs fly at very low altitude) as it would be if satellite data had been used. In addition, the technique when implemented with UAV data, the spatiotemporal variability of EF and M_o are computed at a very fine spatial resolution (at 4 cm in our case). As information on very high spatial and potentially temporal resolution of EF and SSM is essential to decision-making in most agricultural applications, including precision agriculture (Wang et al. 2018; Cui et al. 2020), the potential added value of the 'simplified' triangle technique to addressing this requirement is clear. In overall, all the above characteristics place the 'simplified triangle' in a privileged position as a candidate for further investigation for a potential operationalization with either with satellite or airborne EO data.

6. Conclusions

In this study, a first assessment of the so-called 'simplified triangle' technique was performed to evaluate the ability of this method to predict EF and M_o /SSM when very high spatial resolution EO imagery acquired from UAV are available. A robust evaluation was carried out for an experimental site located in Sicily, Italy for which an extensive field campaign took place in July 2019. To our knowledge, the study represents the first detailed assessment of this innovative method with UAV data, particularly in a Mediterranean setting. The implementation of the investigated herein technique with UAV images presents several advantages. Data cloud cover is not an issue for UAV images and the spatiotemporal variability of EF and M_o /SSM are computed at a very fine spatial resolution (at 4 cm in our case). Regardless, UAV images present an additional challenge in correctly implementing the 'simplified triangle' technique. The method requires a sufficient variability of F_r and SSM range within the image which can prove challenging in UAV imagery.

The obtained results suggest that the 'simplified triangle' performed satisfactorily in predicting both the M_o /SSM and EF. Validation showed an average error of 0.053 for EF and of $0.040 \text{ cm}^3 \text{ cm}^{-3}$ for SSM. This implies that the investigated approach performs well under the semi-arid conditions characterizing the experimental set up. Both predicted maps also exhibited sensible spatial variability across the experimental site, with patterns in agreement to land cover type, topography and other site-specific characteristics. The prediction accuracy of the technique was also in close agreement, or even better, than accuracies reported by other independent investigators using different T_s /VI approaches and EO data types.

However, the results reported herein are evidently based on a single image analysis. As the technique is recent, further scrutiny and additional studies are required to establish its applicability to different ecosystems. Such future investigations would require exploring the prediction accuracy of the technique in different ecosystem environments and for longer time periods using UAV imagery and spaceborne datasets from appropriate sensors (e.g. Landsat, Setinel 1 to 3, Moderate Resolution Imaging Spectroradiometer (MODIS)), as well as including a flux footprint analysis comparisons for the case of EF/ET predictions. In addition, a detailed sensitivity analysis of the method would also allow quantifying the effect of T_s and F_r errors on

prediction accuracy. Other aspects of the technique that deserved investigation involve automating the process of determining the wet and dry edge, which would also eliminate user subjectivity in the technique implementation. It could potentially prove beneficial to combine pixels to satellite sensor spatial resolution (e.g. from the Landsat resolution of 30 or 120 m) to define the triangle boundaries. Then, once those boundaries have been established, they could be imposed on the higher resolution UAV image. All the above are topics of key importance that will be pursued in future studies.

Acknowledgements

Participation of Dr. Petropoulos has been funded by the ENViSioN-EO Marie Skłodowska-Curie grant (grant No 752094), part of the European Union's Horizon 2020 research and innovation programme. Part of the present collaborative work was also materialised in the framework of a short Term Scientific Mission (STSM) of the HARMONIOUS Cost Action which financially supported Dr Petropoulos' visit between 4 to 15 February 2020 to the Department of Engineering of the University of Palermo, Italy. Authors thank also Dr. Mauro Lo Brutto for his help in collecting the GNSS data.

Author contributions

AM, GP, GC, and SM conceived and planned the experiments. AM and FC contributed to the experimental design of the spectroradiometric acquisitions and radiometric calibration of the images. GC, GP and SM coordinated the experiment and provided instrumentations. AM and GD contributed to the GNSS experimental design and processing. GP contributed to the experimental design and management of the soil moisture probes and processed the data. AM processed the flux tower data. SM and FC designed and acquired the UAV images. GPP, AP, TNC, DH and CC contributed to model implementation, results processing and analysis. GPP, AP prepared the original draft of the manuscript. All authors reviewed and edited the final version of the manuscript and contributed to the preparation of the revised manuscript.

Authors' Initials are defined as follows

George P. Petropoulos (GPP), Antonino Maltese (AM), Toby N. Carlson (TNC), Giuseppe Provenzano (GP), Andrew Pavlides (AP), Giuseppe Ciruolo (GC), Dionissios Hristopoulos (DH), Fulvio Capodici (FC), Christos Chalkias (CC), Gino Dardanelli (GD), Salvatore Manfreda (SM).

Disclosure statement

No potential conflict of interest was reported by the authors.

Funding

This work was supported by the FP7 People: Marie-Curie Actions [752094].

References

- Amani, M., S. Parsian, S. M. Mirmazloumi, and O. Aieneh. 2016. "Two New Soil Moisture Indices Based on the NIR-red Triangle Space of Landsat-8 Data." *International Journal of Applied Earth Observation & Geoinformation* 50: 176–186. doi:10.1016/j.jag.2016.03.018.
- Angrisano, A., G. Dardanelli, A. Innac, A. Pisciotta, C. Pipitone, and S. Gaglione. 2020. "Performance Assessment of PPP Surveys with Open Source Software Using the GNSS GPS–GLONASS–Galileo Constellations." *Applied Sciences* 10 (16): 5420. doi:10.3390/app10165420.
- Bai, J. Q. C., W. Zhang, and L. Meng. 2019. "An Approach for Downscaling SMAP Soil Moisture by Combining Sentinel-1 SAR and MODIS Data." *Remote Sensing MDPI* 11 (2736): 1–20.
- Bao, Y., L. Lin, S. Wu, K. A. K. Deng, and G. P. Petropoulos. 2018. "Surface Soil Moisture Retrievals over Partially Vegetated Areas from the Synergy of Sentinel-1 & Landsat 8 Data Using a Modified Water-Cloud Model." *International Journal of Applied Earth Observation & Geoinformation* 72: 76–85. doi:10.1016/j.jag.2018.05.026.
- Barreca, G., V. Bruno, G. Dardanelli, F. Guglielmino, L. O. Brutto, M. Mattia, M. Pipitone, and C. Rossi. 2020. "An Integrated Geodetic and InSAR Technique for the Monitoring and Detection of Active Faulting in Southwestern Sicily." *Annals of Geophysics* 63: art. no. EP03. doi:10.4401/ag-8327.
- Capodici, F., C. Cammalleri, A. Francipane, G. Ciraolo, G. La Loggia, and A. Maltese. 2020. "Soil Water Content Diachroni Mapping: An FFT Frequency Analysis of a Temperature-Vegetation Index." *Geosciences MDPI* 10 (23): 1–18.
- Carlson, T. N. 2007. "An Overview of the "Triangle Method" for Estimating Surface Evapotranspiration and Soil Moisture from Satellite Imagery." *Sensors MDPI* 7 (8): 1612–1629. doi:10.3390/s7081612.
- Carlson, T. N., and G. P. Petropoulos. 2019. "A New Method for Estimating of Evapotranspiration and Surface Soil Moisture from Optical and Thermal Infrared Measurements: The Simplified Triangle." *International Journal of Remote Sensing* 40 (20): 7716–7729. doi:10.1080/01431161.2019.1601288.
- Catania, P., A. Comparetti, P. Febo, G. Morello, S. Orlando, E. Roma, and M. Vallone. 2020. "Positioning Accuracy Comparison of GNSS Receivers Used for Mapping and Guidance of Agricultural Machines." *Agronomy* 10 (7): art. no. 924. doi:10.3390/agronomy10070924.
- Chauhan, N. S., S. Miller, and P. Ardanuy. 2003. "Spaceborne Soil Moisture Estimation at High Resolution: A microwave-optical/IR Synergistic Approach." *International Journal of Remote Sensing* 22: 4599. doi:10.1080/0143116031000156837.
- Cui, Y., S. Ma, Z. Yao, X. Chen, Z. Luo, W. Fan, and Y. Hong. 2020. "Developing a Gap-filling Algorithm Using DNN for the T_s/VI Triangle Model to Obtain Temporally Continuous Daily Actual Evapotranspiration in an Arid Area of China." *Remote Sensing MDPI* 12 (1221): 1–17.
- Dardanelli, G., La Loggia, G. Perfetti, N. Capodici, F. Puccio, and L. Maltese. 2014. "Monitoring Displacements of an Earthen Dam Using GNSS and Remote Sensing." *Proceedings of SPIE – the International Society for Optical Engineering* 9239: art. no. 923928.
- Dardanelli, G., and M. Carella. 2013. "Integrated Surveying with Mobile Mapping System, EGNOS, NRTK and Laser Technologies in the Park "Ninni Cassarà" in Palermo." *ISPRS Annals of the Photogrammetry, Remote Sensing and Spatial Information Sciences* 2 (2W1): 95–100. doi:10.5194/isprsannals-II-2-W1-95-2013.
- Dardanelli, G., M. Lo Brutto, and C. Pipitone. 2020. "C.GNSS CORS Network of the University of Palermo: Design and First Analysis of Data." *Geographia Technica* 15 (1): 43–69. doi:10.21163/GT_2020.151.05.
- Dardanelli, G., S. Paliaga, M. Allegra, M. Carella, and V. Giammarresi. 2015. "Geomatic Applications Tourban Park in Palermo." *Geographia Technica* 10 (1): pp. 28–43.
- Dawson, R., G. P. Petropoulos, L. Toullos, and P. K. Srivastava. 2019. "Mapping and Monitoring of the Land Use/Cover Changes in the Wider Area of Ltanos, Crete, Using Very High Resolution EO Imagery with Specific Interest in Archaeological Sites." *Environment, Development and Sustainability*. [in press]. doi:10.1007/s10668-019-00353-0.
- Deng, K. A. K., S. Lamine, A. Pavlides, G. P. Petropoulos, Y. Bao, P. K. Srivastava, and Y. Guan. 2019. "Large Scale Operational Soil Moisture Mapping from Passive MW Radiometry: SMOS Product

- Evaluation in Europe & USA." *International Journal of Applied Earth Observation & Geoinformation* 80: 206–217. doi:[10.1016/j.jag.2019.04.015](https://doi.org/10.1016/j.jag.2019.04.015).
- Finn, M. P., M. Lewis, D. D. Bosch, M. Giraldo, K. Yamamoto, D. G. Sullivan, and M. S. Williams. 2011. "Remote Sensing of Soil Moisture Using Airbornehyperspectral Data." *GISci. Remote Sens* 48 (4): 522–540. doi:[10.2747/1548-1603.48.4.522](https://doi.org/10.2747/1548-1603.48.4.522).
- Fuzzo, S. D., T. N. Carlson, N. Kourgiyalas, and G. P. Petropoulos. 2020. "Coupling Remote Sensing with a Water Balance Model for Soybean Yield Predictions over Large Areas." *Earth Science Informatics* 13, pages 345–359(2020).
- Gerken, T., B. L. Ruddell, R. Yu, P. C. Stoy, and D. T. Drewry 2019. "Robust Observations of Land-to-atmosphere Feedbacks Using the Information Flows of FLUXNET." *Npj Climate and Atmospheric Science* 2 (37). doi:[10.1038/s41612-019-0094-4](https://doi.org/10.1038/s41612-019-0094-4).
- Gillies, R. R., T. N. Carlson, J. Cui, W. P. Kustas, and K. S. Humes. 1997. "Verification of the "Triangle" Method for Obtaining Surface Soil Water Content and Energy Fluxes from Remote Measurements of the Normalized Difference Vegetation Index NDVI and Surface Radiant Temperature." *International Journal of Remote Sensing* 18: 3145–3166. doi:[10.1080/014311697217026](https://doi.org/10.1080/014311697217026).
- Granier, A. 1985. "Une nouvelle methode pour la mesure du flux de seve brute dans le tronc des arbres." *Annales des Sciences Forestières* 42: 193–200. doi:[10.1051/forest:19850204](https://doi.org/10.1051/forest:19850204).
- Harwin, S., and A. Lucieer. 2012. "Assessing the Accuracy of Georeferenced Point Clouds Produced via Multi-view Stereopsis from Unmanned Aerial Vehicle (UAV) Imagery." *Remote Sensing MDPI* 4 (6): 1573–1599. doi:[10.3390/rs4061573](https://doi.org/10.3390/rs4061573).
- Ireland, G., G. P. Petropoulos, T. N. Carlson, and S. Purdy. 2015. "Addressing the Ability of a Land Biosphere Model to Predict Key Biophysical Vegetation Characterisation Parameters with Global Sensitivity Analysis." *Environmental Modelling and Software* 65: 94–107. doi:[10.1016/j.envsoft.2014.11.010](https://doi.org/10.1016/j.envsoft.2014.11.010).
- Jung, M., M. Reichstein, H. A. Margolis, A. Cescatti, A. D. Richardson, M. A. Arain, ... C. Williams. 2011. "Global Patterns of Land-atmosphere Fluxes of Carbon Dioxide, Latent Heat, and Sensible Heat Derived from Eddy Covariance, Satellite, and Meteorological Observations." *Journal of Geophysical Research: Biogeosciences* 116: G3.
- Karpouzli, E., and T. Malthus. 2003. "The Empirical Line Method for the Atmospheric Correction of IKONOS Imagery." *International Journal of Remote Sensing* 24 (5): 1143–1150. doi:[10.1080/0143116021000026779](https://doi.org/10.1080/0143116021000026779).
- Kasim, A. A., T. N. Carlson, and H. S. Usman. 2020. "Limitations in Validating Derived Soil Water Content from Thermal/optical Measurements Using the Simplified Triangle Method." *Remote Sensing, MDPI* 12 (1155): 1–15.
- Kenyeres, A., J. G. Bellet, C. Bruyninx, A. Caporali, F. De Doncker, B. Droscak, A. Duret, et al. 2019. "Regional Integration of Long-term National Dense GNSS Network Solutions." *GPS Solutions* 23 (4): art. no. 122. doi:[10.1007/s10291-019-0902-7](https://doi.org/10.1007/s10291-019-0902-7).
- Liu, Y., W. Jing, Q. Wang, and X. Xia. 2020. "Generating High-resolution Daily Soil Moisture by Using Spatial Downscaling Techniques: A Comparison of Six Machine Learning Algorithms." *Advances in Water Resources* 141: 103601–103623. doi:[10.1016/j.advwatres.2020.103601](https://doi.org/10.1016/j.advwatres.2020.103601).
- Lu, J., R. Tang, K. Shao, Z. L. Li, and G. Zhou. 2015. "Assessment of Two Temporal-information-based Methods for Estimating Evaporative Fraction over the Southern Great Plains." *International Journal of Remote Sensing* 36 (19-20), 1–17.
- Maltese, A., F. Capodici, G. Ciraolo, and G. La Loggia. 2015. "Soil Water Content Assessment: Critical Issues Concerning the Operational Application of the Triangle Method." *Sensors MDPI* 15 (3): 6699–6719. doi:[10.3390/s150306699](https://doi.org/10.3390/s150306699).
- Maseroli, R. 2015. "Evoluzione del Sistema Geodetico di Riferimento in Italia: La RDN2." *Bollettino della Associazione Italiana di Cartografia* 153: 19–44.
- Mi, S., H. Su, R. Zhang, and J. Tian. 2015. "Using Simplified Thermal Inertia to Determine the Theoretical Dry Line in Feature Space for Evapotranspiration Retrieval." *Remote Sensing MDPI* 7 (8): 10856–10877. doi:[10.3390/rs70810856](https://doi.org/10.3390/rs70810856).
- Minacapilli, M. S., D. V. Consoli, G. Ciraolo, and A. Motisi. 2016. "A Time Domain Triangle Method Approach to Estimate Actual Evapotranspiration: Application in A Mediterranean Region Using

- MODIS and MSG-Seviri Products." *Remote Sensing of Environment* 174: 10–23. doi:10.1016/j.rse.2015.12.018.
- Negm, A., F. Capodici, G. Ciraolo, A. Maltese, G. Provenzano, and G. Rallo. 2017. "Assessing the Performance of Thermal Inertia and Hydrus Models to Estimate Surface Soil Water Content." *Applied Science* 7(10), 975.
- North, M. R., G. P. Petropoulos, D. V. Rentall, G. I. Ireland, and J. P. Mccalmonth. 2015. "Appraising the Capability of a Land Biosphere Model as a Tool in Modelling Land Surface Interactions: Results from Its Validation at Selected European Ecosystems." *Earth Surface Dynamics Discussions* 6: 217–265. doi:10.5194/esdd-6-217-2015.
- Nutini, F., M. Boschetti, G. Candiani, S. Bocchi, and P. A. Brivio. 2014. "Evaporative Fraction as an Indicator of Moisture Condition and Water Stress Status in Semi-arid Rangeland Ecosystems." *Remote Sensing MDPI* 6 (7): 6300–6323. doi:10.3390/rs6076300.
- Peng, J., and A. Loew. 2014. "Evaluation of Daytime Evaporative Fraction from MODIS TOA Radiances Using Fluxnet Observations." *Remote Sensing, MDPI* 6 (7): 5959–5975. doi:10.3390/rs6075959.
- Petropoulos, G. P., T. N. Carlson, and H. Griffiths. 2013. "Turbulent Fluxes of Heat and Moisture at the Earth's Land Surface: Importance, Controlling Parameters and Conventional Measurement, Chapter 1, Pages 3–28." In *Remote Sensing of Energy Fluxes and Soil Moisture Content*. edited by G. P. Petropoulos. ISBN: 978–1–4665–0578–0, p. 3–28. Boca Raton, FL: Taylor & Francis.
- Petropoulos, G. P., G. Ireland, and B. Barrett. 2015. "Surface Soil Moisture Retrievals from Remote Sensing: Current Status, Products & Future Trends." *Physics and Chemistry of the Earth* 83–84: 36–56. [in press]. doi:10.1016/j.pce.2015.02.009.
- Petropoulos, G. P., P. K. Srivastava, K. P. Feredinos, and D. Hristopoulos. 2018. "Evaluating the Capabilities of optical/TIR Imagine Sensing Systems for Quantifying Soil Water Content." *Geocarto International*. doi:10.1080/10106049.2018.1520926.
- Petropoulos, G. P., T. N. Carlson, M. J. Wooster, and S. Islam. 2009. "A Review of T_s/VI Remote Sensing Based Methods for the Retrieval of Land Surface Fluxes and Soil Surface Moisture Content." *Advances in Physical Geography* 33 (2): 1–27.
- Piles, M., G.P. Petropoulos, N. Sanchez, A. González-Zamora & G. Ireland. (2016). Towards Improved Spatio-Temporal Resolution Soil Moisture Retrievals From the Synergy of SMOS & MSG SEVIRI Spaceborne Observations. *Remote Sensing of Environment*, 180, pp:403-471. doi: 10.1016/j.rse.2016.02.048
- Pipitone, C., A. Maltese, G. Dardanelli, M. L. Brutto, and G. La Loggia. 2018. "Monitoring Water Surface and Level of a Reservoir Using Different Remote Sensing Approaches and Comparison with Dam Displacements Evaluated via GNSS." *Remote Sensing* 10 (1): art. no. 71.
- Scholander, P. F., H. J. Hammel, A. Bradstreet, and E. A. Hemmingsen. 1965. "Sap Pressure in Vascular Plants." *Science* 148: 339–346. doi:10.1126/science.148.3668.339.
- Schuepp, P. H., M. Y. Leclerc, J. I. Macpherson, and R. L. Desjardins. 1990. "Footprint Prediction of Scalar Fluxes from Analytical Solutions of the Diffusion Equation." *Bound.-Layer Meteorol* 1990 (50): 355–373. doi:10.1007/BF00120530.
- Shi, Q., and S. Liang. 2014. "Surface-sensible and Latent Heat Fluxes over the Tibetan Plateau from Ground Measurements, Reanalysis, and Satellite Data." *Atmospheric Chemistry and Physics* 14 (11): 5659–5677. doi:10.5194/acp-14-5659-2014.
- Sobrinho, J. A., J. C. Jimenez-Munoz, and L. Paolini. 2004. "Land Surface Temperature Retrieval from LANDSAT TM 5." *Remote Sensing of Environment* 90 (2004): 434–440. doi:10.1016/j.rse.2004.02.003.
- Srivastava, P. K., D. HAN, T. Islam, G. P. Petropoulos, M. & Gupta, and Q. Dai. 2015. "Seasonal Evaluation of Evapotranspiration Fluxes from MODIS Satellite and Mesoscale Model Downscaled Global Reanalysis Datasets." *Theoretical and Applied Climatology* 1–14. doi:10.1007/s00704-015-1430-1.
- Srivastava, P. K., P. C. Pandey, G. P. Petropoulos, N. K. Kourgialas, S. Pandley, and U. Singh. 2019. "GIS and Remote Sensing Aided Information for Soil Moisture Estimation: A Comparative Study of Interpolation Technique." *Resources MDPI* 8 (2): 70. doi:10.3390/resources8020070.

- Tang, R., and Z. L. Li. 2017. "An End-Member-Based Two-Source Approach for Estimating Land Surface Evapotranspiration from Remote Sensing Data." *IEEE Transactions on Geoscience and Remote Sensing* 55 (10): 5818–5832. doi:[10.1109/TGRS.2017.2715361](https://doi.org/10.1109/TGRS.2017.2715361).
- Tian, F., G. Qiu, Y. Lü, Y. Yang, and Y. Xiong. 2014. "Use of High-resolution Thermal Infrared Remote Sensing and "Three-temperature Model" for Transpiration Monitoring in Arid Inland River Catchment." *Journal of Hydrology* 515: 307–315. doi:[10.1016/j.jhydrol.2014.04.056](https://doi.org/10.1016/j.jhydrol.2014.04.056).
- Tomas, D. E. A., H. Mnieto, R. Guzinski, J. Salas, I. Sandholt, and P. Berliner. 2014. "Validation and Scale Dependencies of the Triangle Method for the Evaporative Fraction Estimation over Heterogeneous Areas." *Remote Sensing of Environment* 151: 493–511. doi:[10.1016/j.rse.2014.06.028](https://doi.org/10.1016/j.rse.2014.06.028).
- Valor, E., and V. Caselles. 1996. "Mapping Land Surface Emissivity from NDVI: Application to European, African, and South American Areas." *Remote Sensing of Environment* 57: 167–184. doi:[10.1016/0034-4257\(96\)00039-9](https://doi.org/10.1016/0034-4257(96)00039-9).
- Wang, S., M. Garcia, A. Ibrom, J. Jakobsen, C. J. Koppl, K. Mallick, M. C. Looms, and P. Bauer-Gottwein. 2018. "Mapping Root Zone Soil Moisture Using a Temperature-vegetation Triangle Approach with an Unmanned Aerial System: Incorporating Surface Roughness from Structure from Motion." *Remote Sensing MDPI* 10 (1978): 1–28.
- Xu, C., J. J. Qu, X. Hao, M. H. Cosh, J. H. Prueger, Z. Zhu, and L. Gutenberg. 2018. "Downscaling of Surface Soil Moisture Retrieval by Combining MODIS/Landsat and In-situ Measurements." *Remote Sensing MDPI* 10 (210): 1–16.
- Zhang, D., R. Tang, W. Zhao, B. Tang, H. Wu, K. Shao, and Z. L. Li. 2014. "Surface Soil Water Content Estimation from Thermal Remote Sensing Based on the Temporal Variation of Land Surface Temperature." *Remote Sensing MDPI* 6 (4): 3170–3187. doi:[10.3390/rs6043170](https://doi.org/10.3390/rs6043170).